Int. J. Heat Mass Transfer. Vol. 36, No. 8, pp. 2083–2092, 1993
Printed in Great Britain

0017-9310/93 $6.00+0.00

Study of the heat transfer behavior of a latent heat thermal energy storage unit with a finned tube

MARCEL LACROIX
Département de génie mécanique, Université de Sherbrooke, Sherbrooke (Québec), Canada J1K 2R1

(*Received* 8 *June* 1992 *and in final form* 19 *October* 1992)

Abstract—A theoretical model for predicting the transient behavior of a shell-and-tube storage unit with the PCM on the shell side and the HTF circulating inside the tubes is presented. The tubes are bare or finned. The multidimensional phase change problem is tackled with an enthalpy based method coupled to the convective heat transfer from the HTF. The numerical model is validated with experimental data. A series of numerical experiments are then undertaken to assess the effects of (1) the shell radius, (2) the mass flow rate and inlet temperature of the HTF and (3) the presence of fins attached to the inner tubes on the thermal behavior of the thermal unit. Results show that the annular fins are most effective for moderate mass flow rates and small inlet temperatures.

INTRODUCTION

IN RECENT years, thermal storage units that utilize latent heat of storage materials have received increasing research attention because they offer advantages over materials whose thermal storage capacity is based exclusively on sensible heat. Many theoretical studies concerning the thermal characteristics of heat exchangers based on Phase Change Materials (PCMs) have been undertaken. Such studies constitute an integral part of analyzing and optimizing the design of latent heat storage systems.

A latent heat storage system which promises high efficiency for a minimum volume is the shell-and-tube type of exchanger with the PCM filling the shell-side while the heat transfer fluid (HTF) flows through the tubes and serves to convey the stored energy to and from the storage unit. This type of latent heat storage unit has been studied by several authors using mathematical models of different complexity [1–3]. In some models [2], the thermal resistance of the PCM was ignored (the Biot number is negligibly small) while in others [1–3] heat conduction parallel to the tube axes and the effects of axial changes in the temperature of the heat transfer fluid were omitted. More recently, a theoretical model of a shell-and-tube PCM storage unit was reported by Ismail and Alves [4]. In this model, the energy equation for the PCM was written in terms of the enthalpy. The numerical results showed the effects of the Biot number, of the relative diameters of the tubes as well as of the inlet fluid temperature on the thermal performance of the unit. Yimmer and Adami [5] also developed a numerical model for optimizing a basic one-dimensional shell-and-tube thermal energy storage system. Again, an enthalpy approach was adopted for the PCM. A parametric study was then conducted in order to assess the effects of the inner tube and outer shell radii and of the liquid phase thermal conductivity of the PCM on the performance of the unit.

All the aforementioned studies considered essentially the one-dimensional (radial direction only) phase change problem or the one-dimensional problem of convective heat transfer between the HTF and the PCM. None of these studies dealt with more realistic and more complicated time-dependent multidimensional phase change problem. Indeed, as the HTF flows through the tubes, it exchanges heat with the PCM and experiences changes in the bulk temperature which, in turn, affect the phase change process in the PCM.

Another important aspect of latent heat thermal storage materials, which is also a significant drawback, is their low thermal conductivity (low thermal diffusivity). Although several methods to enhance transfer in latent heat thermal energy storage systems have been proposed [6], the use of finned tubes is considered to be especially effective and reliable. Few studies on the utilization of fins have been reported [7–10]. Sasaguchi and co-workers [7] conducted an experimental and a theoretical study on the effects of the configuration of a finned tube on the heat transfer characteristics of a latent heat thermal energy storage unit. Sasaguchi [8] later carried out a three-dimensional numerical calculation to obtain the performance of a longitudinal finned-tube latent heat storage unit. The effects of various parameters, i.e. the *NTU* and Biot numbers, on the heat transfer process were examined. For simplicity however, no subcooling of the PCM was allowed. Padmanabhan and Murthy [9] presented a theoretical analysis for the transient, solid–liquid phase change process occurring

NOMENCLATURE

C_c heat capacity of HTF [J kg^{-1} K^{-1}]
C_f heat capacity of fins [J kg^{-1} K^{-1}]
C_k heat capacity of phase k in PCM [J kg^{-1} K^{-1}]
C_1 constant (equation 1)
f liquid fraction of the melt
h volumetric enthalpy [J m^{-3}]
HTF heat transfer fluid or working fluid
k_e effective thermal conductivity [W m^{-1} K^{-1}]
k_l thermal conductivity of the melt [W m^{-1} K^{-1}]
l thickness of fins [m]
L length of thermal unit [m]
$\dot{m}$ mass flow rate [kg s^{-1}]
M number of axial nodes
MVF molten volume fraction
n exponent (equation 1)
N number of radial nodes
PCM phase change material
r radial coordinate [m]
Ra Rayleigh number, $g\beta(T_W - T_m)R_i^3\alpha_l^{-1}\gamma_l^{-1}$
R_e mean radius of outside tube [m]
R_i mean radius of inside tube [m]
t time [s]
T temperature of PCM [K]
T_c temperature of HTF [K]
T_f temperature of fins [K]
$(T_c)_{in}$ inlet temperature of HTF [K]
U convective heat transfer coefficient [W m^{-2} K^{-1}]
z axial coordinate [m].

Greek symbols
α thermal diffusivity [m^2 s^{-1}]
ρ density [kg m^{-3}]
ρ_k density of phase k in the PCM
Δh_{fu} latent heat of fusion [J kg^{-1}]
Δr space increment in radial direction [m]
Δt time step [s]
ΔT_{in} $(T_c)_{in} - T_m$
Δz space increment in axial direction [m].

Subscripts
c heat transfer fluid
f fins
l liquid phase
m melting temperature
s solid phase
W, E, P, N, S West, East, Center, North and South nodes
w, e, n, s west, east, north and south faces of control volumes.

in a cylindrical annulus in which rectangular circumferential fins are attached to the inner tube. The inner tube was maintained at a constant temperature and the fins extended from the inner tube to the outer tube. Natural convection effects were ignored and a Landau transformation was adopted for immobilizing the moving solid–liquid interface. Eftekhar *et al.* [10] reported an experimental study of heat transfer enhancement in a paraffin wax thermal storage system consisting of vertically arranged fins between a heated and cooled horizontal finned-tube arrangement.

In the present study, the phase change problem of the PCM around a finned tube is analyzed in terms of both radial and axial directions and is linked to the convective heat transfer from the HTF. In this case, the unknown tube wall temperature is assumed to be time and location dependent. The problem is rather difficult to solve because of the moving boundary and the unknown wall temperature. By introducing an enthalpy-based method, the phase change problem becomes more tractable: the governing enthalpy equation is similar to the single-phase energy equation. The unknown tube wall temperature between the HTF and the PCM is obtained from an energy balance at the wall. An iterative solution method is, however, required.

The objectives of this paper are twofold: first, a computational methodology is presented (and validated with experimental data) for predicting the heat transfer between the HTF and the PCM of a shell-and-tube latent heat storage unit with finned tubes and second, parametric studies are performed in order to assess the effects of various thermal and geometric parameters on the heat-transfer process and on the behavior of the system.

ANALYTICAL MODEL

The shell-and-tube PCM storage unit considered in the present study is shown in Fig. 1. The PCM fills the shell space while the heat transfer fluid flows inside the tubes of radius R_i. The tubes are staggered so that around each of them there is a boundary (dotted lines) across which the conduction heat fluxes remain null. This region of symmetry may be bounded approximately by a radius R_e. As a result, the physical system to be analyzed here may be represented by the simpler geometry shown in Fig. 2. In addition, the following assumptions are made:

1. The thermophysical properties of the PCM and of the working fluid are independent of temperature. They may, however, for the PCM, be different in the solid and liquid phases.

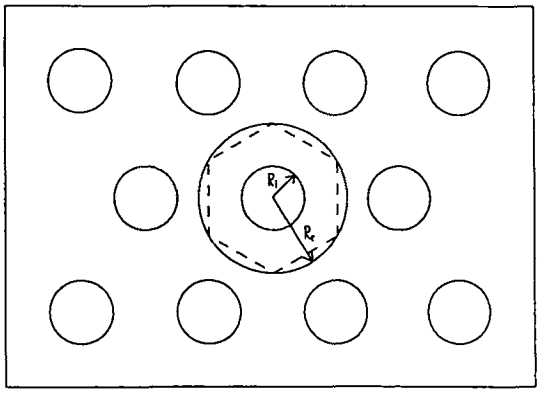

FIG. 1. Staggered arrangement of tubes.

2. The PCM is homogeneous and isotropic.
3. Heat conduction is axisymmetric around the inside tube.
4. The thermal resistance across the inside tube surface is negligible.
5. The fins are sufficiently thin so that their temperature can be considered to be a function of the radius r and time t.
6. The local convective heat transfer coefficient for the HTF may vary along the tube.

The third assumption is retained mainly to avoid the tedious and time-consuming solution of the complete set of multidimensional convective heat transfer equations for the PCM [11]. The effect of natural convection in the melt is, however, included in the conduction equation by employing an effective thermal conductivity k_e for the liquid using the following empirical correlation [12]:

$$k_e/k_l = C_l Ra^n \tag{1}$$

where C_l and n are constants to be determined experimentally.

Subjected to the foregoing assumptions, the conservation equations governing heat transfer are:

for the PCM,

$$\frac{\partial h}{\partial t} = \frac{1}{r}\frac{\partial}{\partial r}\left(\alpha r \frac{\partial h}{\partial r}\right) + \frac{\partial}{\partial z}\left(\alpha \frac{\partial h}{\partial z}\right) - \rho \Delta h_{fu} \frac{\partial f}{\partial t} \tag{2}$$

for the HTF,

$$\rho_c C_c \pi R_i^2 \frac{\partial T_c}{\partial t} = 2\pi R_i U(T - T_c) - \dot{m} C_c \frac{\partial T_c}{\partial z} \tag{3}$$

for the fins,

$$\frac{\partial T_f}{\partial t} = \frac{1}{r}\frac{\partial}{\partial r}\left(\alpha_f r \frac{\partial T_f}{\partial r}\right) + \frac{1}{\rho_f C_f l}\left(\left(k_e \frac{\partial T}{\partial Z}\right)_{left} + \left(k_e \frac{\partial T}{\partial Z}\right)_{right}\right). \tag{4}$$

The enthalpy equation (2) follows Crank's formulation [13] for which the total enthalpy is split into sensible and latent heat components, that is

$$H(T) = h(T) + \rho_s f \Delta h_f$$

where

$$h(T) = \int_{T_m}^{T} \rho_k C_k \, dT \tag{5}$$

ρ_k is the phase density, C_k is the phase specific heat, T_m is the phase change temperature and f is the local liquid fraction. The potential advantage of this formulation is that the enthalpy equation is cast in a standard form with the problems associated with the phase change isolated in a source term.

Equation (4) states that the fin temperature distribution $T_f(t, r)$ is not preassigned, but varies along the height (i.e. as a function of r) in accordance with the conservation laws. However, for the simulation of the melting process, the temperature variation along the fins is practically imperceptible as heat is diffused about 500 times faster in copper than in paraffin (ratio of thermal diffusivities). Nonetheless, the temperature distribution for each fin is different and time dependent as the base temperature is correlated via a boundary condition to the HTF temperature $T_c(t, z)$ which in turn varies along the inside tube. The last term on the right hand side of equation (4) represents the heat transfer from both surfaces of the fin (left and right surfaces) to the surrounding PCM.

The boundary conditions may be stated as:

at the inlet ($z = 0$):

$$\frac{\partial h}{\partial z} = 0; \quad T_c = (T_c)_{in} \tag{6a}$$

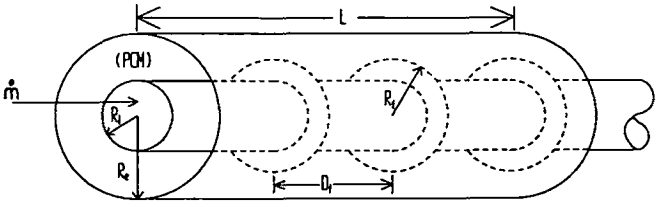

FIG. 2. Schematic representation of the unit.

at the outlet ($z = L$):

$$\frac{\partial h}{\partial z} = 0 \tag{6b}$$

at $r = R_i$:

$$k_c \frac{\partial T}{\partial r} = U(T - T_c); \quad k_f \frac{\partial T_f}{\partial t} = U(T_f - T_c) \tag{6c}$$

at $r = R_c$:

$$\frac{\partial h}{\partial r} = 0 \tag{6d}$$

at $r = R_f$:

$$\frac{\partial T_f}{\partial r} = 0. \tag{6e}$$

Initially, the PCM, the fins and the HTF are all at the same temperature. The working fluid suddenly undergoes in a transient state for which its inlet temperature and its mass flow rate are given by $(T_c)_{in}$ and $\dot{m}$ respectively.

NUMERICAL SOLUTION

Equations (2)–(4) are solved numerically using a finite difference solution method. The finite difference equation for the PCM is obtained on integrating equation (2) over each of the control volumes in the (r, z) plane. The resulting scheme has the form:

$$A_S h_S + A_W h_W + A_P h_P + A_E h_E + A_N h_N = Q \tag{7}$$

where

$$A_S = -(\alpha r)_s \frac{\Delta z}{\Delta r_s}$$

$$A_N = -(\alpha r)_n \frac{\Delta z}{\Delta r_n}$$

$$A_W = -\alpha_w \bar{r} \frac{\Delta r}{\Delta z_w}$$

$$A_E = -\alpha_e \bar{r} \frac{\Delta r}{\Delta z_e}$$

$$A_P = -A_S - A_N - A_W - A_E + \bar{r} \frac{\Delta z \Delta r}{\Delta t}$$

and

$$\bar{r} = (r_s + r_n)/2. \tag{8}$$

Equation (7) is solved using a tridiagonal matrix algorithm solver (TDMA).

The central feature of the present enthalpy fixed grid technique is the source term Q:

$$Q = \bar{r} \frac{\Delta z \Delta r}{\Delta t} h_P^o + \rho \Delta h_f \frac{\Delta z \Delta r}{\Delta t} (f_P^o - f_P^k). \tag{9}$$

Here, h_P^o and f_P^o represent the enthalpy and the liquid fraction respectively from the previous time step. The last term in equation (9) keeps track of the latent heat evolution and its driving element is the local liquid fraction f. This fraction takes the value of 1 in fully liquid regions, 0 in fully solid regions, and lies in the interval [0, 1] in the vicinity of the phase front. Its value is determined iteratively from the solution of the enthalpy equation. Details concerning the numerical implementation of the present enthalpy method are summarized in ref. [14].

The finite difference equation for the temperature of the heat transfer fluid is obtained on integrating equation (3) in the axial direction. The resulting scheme has the form:

$$(T_c)_P = \frac{\left(\frac{(T_c)_P^o}{\Delta t} + \frac{a(T_c)_W}{\Delta z} + bT_P \right)}{\left(\frac{1}{\Delta t} + \frac{a}{\Delta z} + b \right)} \tag{10}$$

where

$$a = \frac{\dot{m}}{\pi R_i^2 \rho_c}, \quad b = \frac{2U}{\rho_c C_c R_i}.$$

The finite-difference equation for the heat diffusion equation for the fins has the form

$$A_S (T_f)_S + A_P (T_f)_P + A_N (T_f)_N = R \tag{11}$$

where

$$A_S = -(\alpha_f r)_s / \Delta r_s$$

$$A_N = -(\alpha_f r)_n / \Delta r_n$$

$$A_P = -A_S - A_N + \frac{\bar{r} \Delta r}{\Delta t} \tag{12}$$

and

$$R = \bar{r} \frac{\Delta r}{\Delta t} (T_f)_P^n + \frac{\bar{r} \Delta r}{\rho_f C_f l} \left(\left(k_c \frac{\partial T}{\partial Z} \right)_{left} + \left(k_c \frac{\partial T}{\partial Z} \right)_{right} \right). \tag{13}$$

Equation (11) is also solved using a tridiagonal matrix solver (TDMA).

All boundary conditions for the enthalpy equation (7) and the fin temperature equation (11) are discretized using second order centered finite differences. The temperature gradients in the source term (13) are also discretized with second order backward and forward finite differences.

Since the enthalpy equation (7) is closely coupled with the heat transfer fluid temperature equation (10) via the boundary condition (6c), both finite difference equations must be solved iteratively at each time step. For a given time step, convergence is declared at the $k+1$th iteration when:

$$\sum_{i=1}^{M} |(T_c)_P^{k+1} - (T_c)_P^k| \leqslant \varepsilon \tag{14}$$

where the sum is taken over M axial nodes. ε is a very small value ($\sim 10^{-7}$). Normally, no more than five or six iterations are needed to meet this stringent convergence criterion.

Furthermore, in order to verify the numerical solu-

tions obtained, the present calculation procedure keeps track of the overall energy balance. At any time, the change in internal energy of the system must be equal to the total energy supplied or extracted at the surface of the inside tube up to the corresponding time. For the present two-dimensional axisymmetric system, the overall energy balance may be expressed as:

$$2\pi R_i \Delta z \int_0^t \sum_{i=1}^{M} U_i((T_c)_i - T_i)\,dt = 2\pi \Delta z \Delta r \times \sum_{j=1}^{N}\sum_{i=1}^{M} r_j(h_{i,j} - \bar{h}_{i,j}) + \rho \Delta h_f (f_{i,j} - \bar{f}_{i,j}) \quad (15)$$

where $\bar{h}_{i,j}$ and $\bar{f}_{i,j}$ are the initial enthalpy and liquid fraction respectively. The left-hand side of equation (15) represents the energy crossing the surface of the inside tube while the right-hand side term represents the stored sensible and latent energy. Both sides are evaluated independently. The convergence criterion ε (equation 14) is chosen so that the numerical deviation between both sides never exceeds 1%.

EXPERIMENTAL APPARATUS AND VALIDATION

The foregoing computational model was first validated with experimental data. To achieve this goal, an experimental storage unit was constructed and experiments were performed. A layout of the storage unit is shown in Fig. 3. It consists essentially of two concentric tubes. The inside tube (0.0127 m i.d., 0.0158 m o.d. and 1.0 m long) is made of copper while the outside tube (0.0258 m i.d. and 1 m long) is made of plexiglass. Twelve equally spaced copper annular fins (0.08 m apart, 0.0256 m outside radius) are soldered to the inside tube. The outside tube is well insulated with thick pipe insulation (Rubatex Armstrong Armflex II). The space between both tubes is filled with *n*-octadecane. Three copper–constantan thermocouples are installed inside the paraffin at various locations shown in Fig. 3. Two additional thermocouples are placed at the inlet and outlet of the inside tube. These thermocouples are connected to a data acquisition system. The heat transfer fluid, i.e. water, from a constant temperature bath is circulated through the copper tube for mass flow rates ranging from 0.03 to 0.07 kg s^{-1}. To minimize the effects of natural convection on the melting, i.e. to maintain the axisymmetric melting around the inside tube, the apparatus is oriented in the vertical direction. Table 1 summarizes the thermophysical properties of *n*-octadecane.

Table 1. Thermophysical properties of *n*-octadecane

fusion temperature	300.7 K
latent heat of fusion	243.5 kJ kg^{-1}
thermal conductivities	
liquid (at 313 K)	0.148 W m^{-1} K^{-1}
solid (at 298 K)	0.358 W m^{-1} K^{-1}
thermal diffusivities	
liquid (at 313 K)	8.64×10^{-8} m^2 s^{-1}
solid (at 298 K)	2.14×10^{-7} m^2 s^{-1}
kinematic viscosity	
liquid (at 313 K)	4.013×10^{-6} m^2 s^{-1}
thermal expansion coefficient	9.0×10^{-4} K^{-1}

Several melting experiments were performed for different mass flow rates and inlet temperatures of the heat transfer fluid. The experiments were first carried out for an inside tube with no fins and then with twelve thin copper fins attached to it. Some results of two of these experiments are reported here, one with no fins and one with twelve fins attached to the inside tube. For both experiments, the mass flow rate and the inlet temperature of the HTF were set to 0.0315 kg s^{-1} and +10 K above the melting point of the

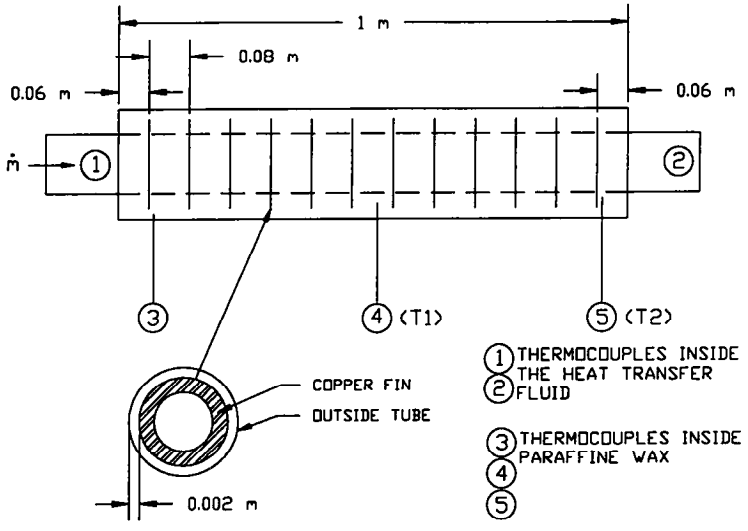

FIG. 3. Experimental test unit.

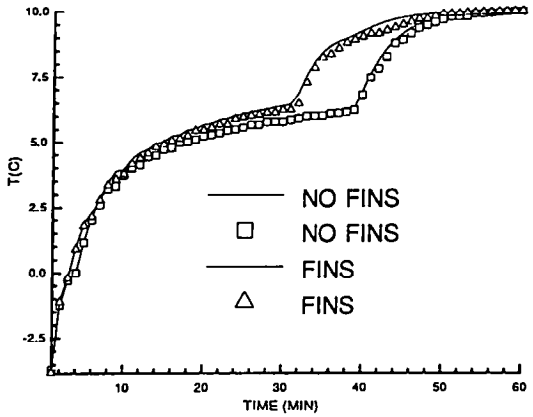

FIG. 4. Numerical predictions (solid lines) and experimental data (symbols) for the timewise variation of the PCM temperature at location T2 (see Fig. 3).

PCM respectively. The initial temperature of the PCM was maintained at 9.5 K (18 K below the melting point of the PCM) by circulating water from a constant temperature bath for a few hours before starting a test run. Once the uniformity of the temperature distribution in the PCM is confirmed within ± 0.1 K, the heat transfer fluid is circulated through the copper tube, and the melting process is initiated.

The computational model was set up to reproduce these experimental conditions. Simulations were carried out for a grid size of 101 nodes in the axial direction and 21 nodes in the radial direction and a fixed time step of 5 s. Figure 4 shows the timewise variations of the predicted and measured values of the temperature at the location T2 ($z = 0.95$ m, $r = 0.001$ m) inside the PCM. The agreement between the predictions and the experimental data is well within the experimental uncertainties. Values of C_1 and n in equation (1) were estimated by comparing the experimental and theoretical results and were found to be 0.099 and 0.25 respectively for the range of mass flow rates and inlet temperatures of the HTF studied. These values are nearly similar to those obtained by Farid and Hussian [12] for the melting of a different commercial n-paraffin wax [7].

NUMERICAL RESULTS

Next, a series of 108 numerical experiments were performed in order to assess the effects of (1) the outside radius R_e, (2) the mass flow rate $\dot{m}(t)$, (3) the inlet temperature of the working fluid $(T_c)_{in}$ and (4) the presence of annular fins on the melting process. The numerical experimental conditions are summarized in Tables 2. The outside radius R_e takes the values of 11 mm, 14.7 mm and 18.3 mm which correspond to a center-to-center distance between the staggered cylinders in a shell-and-tube heat exchanger (Fig. 1) of 19.1 mm, 25.4 mm and 31.7 mm respectively. The thermal unit is still 1 m long and the inside tube radius R_i is also fixed at 6.35 mm. The mass flow rate takes the values of 1.5×10^{-4}, 1.5×10^{-3}, 1.5×10^{-2} and 4.5×10^{-2} kg s^{-1} corresponding to Reynolds flow numbers of 20, 200, 2000 and 6000 respectively. For the laminar flows, i.e. Reynolds number $\leqslant 2000$, it is assumed that the velocity profile

Table 2a. Summary of numerical experiments without fins

R_e [m]	Tag 1	$\dot{m}$ [kg s^{-1}]	Tag 2	ΔT_{in} [K]	Tag 3	Cycle	Tag 4
0.011	a	1.5×10^{-4}	1	5	1		
0.0147	b	1.5×10^{-3}	2	10	2	0-3600-s	1
0.0183	c	1.5×10^{-2}	3	20	3		
		4.5×10^{-2}	4				

Table 2b. Summary of numerical experiments with 12 fins

R_e [m]	Tag 1	$\dot{m}$ [kg s^{-1}]	Tag 2	ΔT_{in} [K]	Tag 3	Cycle	Tag 4
0.011	d	1.5×10^{-4}	1	5	1		
0.0147	e	1.5×10^{-3}	2	10	2	0-3600-s	1
0.0183	f	1.5×10^{-2}	3	20	3		
		4.5×10^{-2}	4				

Table 2c. Summary of numerical experiments with 19 fins

R_e [m]	Tag 1	$\dot{m}$ [kg s^{-1}]	Tag 2	ΔT_{in} [K]	Tag 3	Cycle	Tag 4
0.011	g	1.5×10^{-4}	1	5	1		
0.0147	h	1.5×10^{-3}	2	10	2	0-3600-s	1
0.0183	i	1.5×10^{-2}	3	20	3		
		4.5×10^{-2}	4				

of the working fluid, i.e. water, is fully developed at the inlet while the temperature profile is allowed to develop under a specified wall temperature. As a result, the convective heat transfer coefficient at the wall U (equation (6c)) is estimated at each axial node with a correlation for the local Nusselt number of Graetz solution [15]. For the turbulent flow, i.e. Reynolds number of 6000, a fully developed flow is assumed and the Nusselt number for the working fluid is determined from the Dittus–Boelter correlation [16]. The inlet temperature of the working fluid varies from 5 to 20 degrees above the fusion temperature of the PCM. The melting time is 3600 s and the PCM is *n*-octadecane. For all cases, the initial temperature of the working fluid and of the PCM was set to 10 degrees below the melting point of the PCM.

As an example of the elaborate nomenclature employed in the present study, case No i231 corresponds to a storage unit with 19 annular fins, an outside radius R_e of 0.0183 m (Tag #1), a mass flow rate for the HTF of 1.5×10^{-3} kg s^{-1} (Tag #2), an inlet temperature for the HTF of 20 K above the fusion temperature of the PCM (Tag #3) and a melting cycle of 3600 s (Tag #4).

All numerical experiments were carried out with grid size and time step similar to those employed for the validation experiments. However, few experiments were performed for finer grid sizes and smaller time steps and their predictions did not show noticeable changes with the present results.

Figure 5 shows the timewise variation of the outlet temperature of the HTF for $R_e = 0.011$ m and $R_e = 0.0183$ m respectively. For both figures, the inlet temperature of the HTF was maintained at 20 K above the melting point of the PCM. For the cases at low mass flow rate, i.e. $\dot{m} = 1.5 \times 10^{-4}$ kg s^{-1}, the outlet temperature of the HTF barely exceeds the normalized fusion temperature of the PCM (0 degrees). For experiments a131, d131 and g131, the temperature of the HTF reaches a plateau at the fusion point and stays there for a significant period of time while melting is slowly taking place inside the

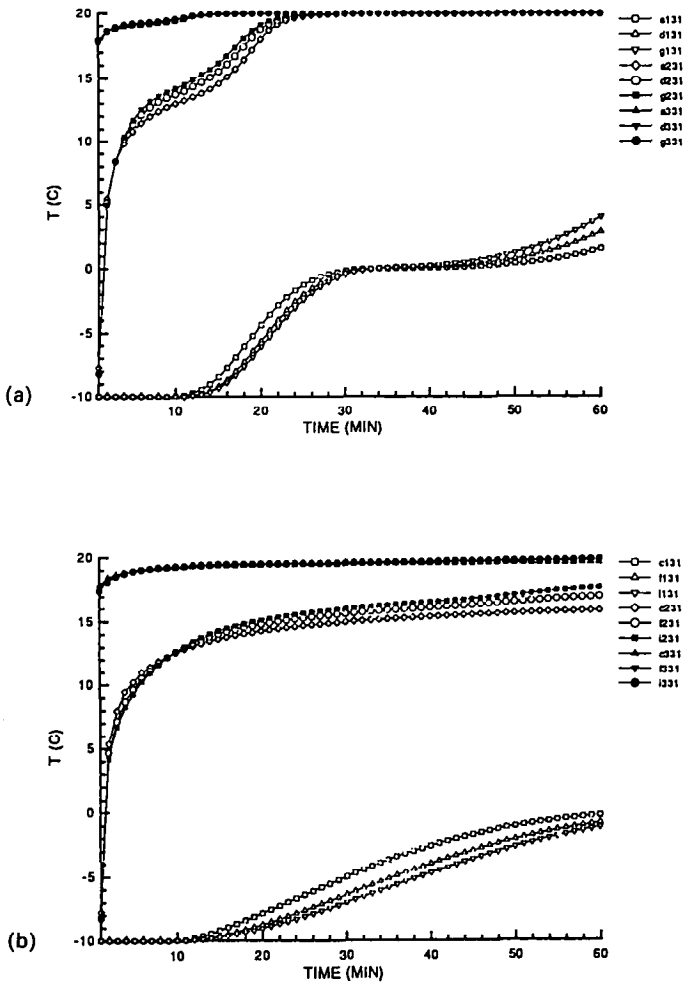

FIG. 5. (a) Timewise variations of the HTF outlet temperature for a shell radius $R_e = 0.011$ m. (b) Timewise variations of the HTF outlet temperature for a shell radius $R_e = 0.0183$ m.

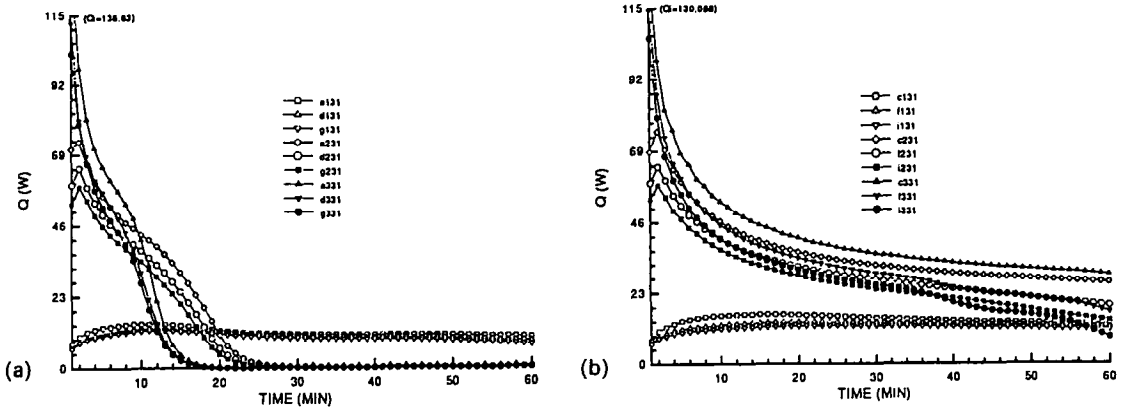

FIG. 6. (a) Timewise variations of the heat transfer rates for a shell radius $R_e = 0.011$ m. (b) Timewise variations of the heat transfer rates for a shell radius $R_e = 0.0183$ m.

PCM. As the external radius of the thermal unit R_e increases, the melting temperature is not even reached (only sensible heat is stored) and its rate of increase becomes smoother. Also, the presence of fins seems to have an opposite effect as for the case with a smaller R_e. For higher mass flow rates however, i.e. $\dot{m} \geqslant 1.5 \times 10^{-3}$ kg s^{-1}, the picture is very different. The outlet temperature quickly reaches a value nearly

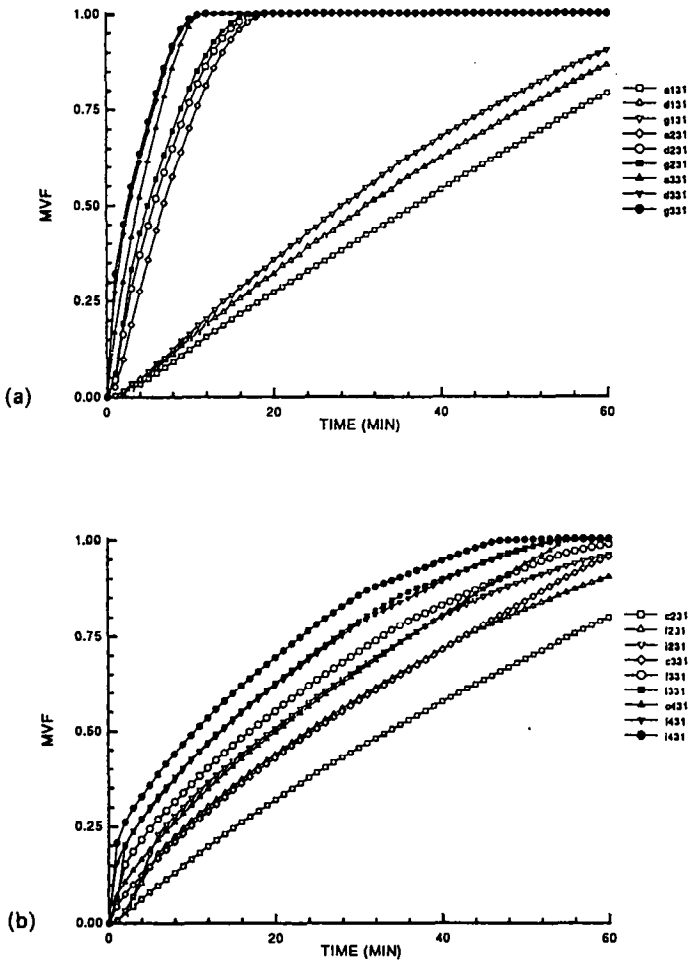

FIG. 7. (a) Timewise variations of the molten volume fractions (MVF) for a shell radius $R_e = 0.011$ m. (b) Timewise variations of the molten volume fractions (MVF) for a shell radius $R_e = 0.0183$ m.

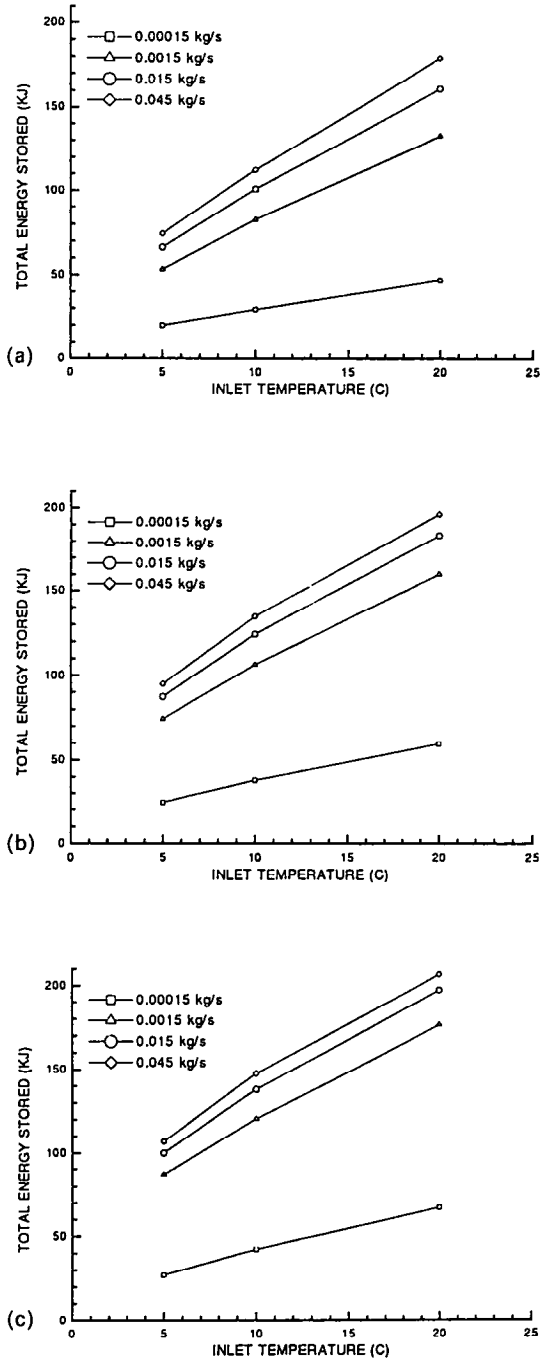

FIG. 8. Total energy stored versus inlet temperature after 45 min for (a) $R_e = 0.0183$ m (no fin) (b) $R_e = 0.0183$ m (12 fins) and (c) $R_e = 0.0183$ m (19 fins).

equal or equal to the inlet temperature. The presence of fins is visible at moderate mass flow rates (1.5×10^{-3} kg s^{-1}) and imperceptible for $\dot{m} \geqslant 1.5 \times 10^{-3}$ kg s^{-1}.

The corresponding timewise variations of the heat transfer rates across the inside tube wall are depicted in Fig. 6. By comparing these results with Fig. 5, it is seen that a decrease of Q closely matches an increase of the outlet temperature. At early times, Q increases, reaches a maximum and then decreases steadily. As $\dot{m}$ increases, the initial rise of Q occurs earlier and for a high mass flow rate it does not even shown on these figures. Also, for high mass flow rates $\dot{m} \geqslant 1.5 \times 10^{-3}$ kg s^{-1} and geometry a (smallest R_e), Q decreases quickly and becomes null after 60 min. Indeed, after that period of time, the PCM is entirely melted and its temperature is nearly uniform and equal to the inlet temperature of the HTF. This is shown in Fig. 7 as the molten volume fractions of the PCM (MVF) are plotted against time. As R_e increases, the decrease of Q becomes smoother and for the largest R_e (geometries c, f and i), it levels off to nearly constant values. In fact, for these geometries, the PCM is entirely melted after 60 min only for cases with the largest mass flow rate of 4.5×10^{-2} kg s^{-1}. The enhancement of the heat transfer rate due to the presence of fins is also clearly seen even for high mass flow rates (Fig. 7(b)).

The total energy stored (latent heat + sensible heat) after 45 min of melting for geometries c, f and i is depicted in Fig. 8. For the range of inlet temperatures and mass flow rates studied, the stored energy varies linearly with the inlet temperature and with an increasing slope for augmenting mass flow rates. The increases in the total energy stored for a storage unit with 12 and 19 fins are summarized in Table 3. The largest increases are obtained for moderate mass flow rates (0.0015 kg $s^{-1} \leqslant m \leqslant 0.015$ kg s^{-1}) and a small inlet temperature ($\Delta T_{in} = +5$ K). The smallest increases are reported for a large mass flow rate ($\dot{m} = 0.045$ kg s^{-1}) and a large inlet temperature ($\Delta T_{in} = +20$ K).

CONCLUDING REMARKS

A theoretical model was developed to predict the transient behavior of a shell-and-tube storage unit with the PCM filling the shell side and the HTF circulating inside the finned tubes. The phase change problem of the PCM around the tubes is treated in both radial and axial directions using an enthalpy based method and is strongly coupled to the convective heat transfer from the HTF. The model also

Table 3. Increase in the total energy stored with a finned tube compared to a bare tube

ΔT_{in} (K)	$\dot{m}$ (kg s^{-1})	12 fins	19 fins
+5	0.00015	25%	40%
+5	0.0015	44%	63%
+5	0.015	31%	54%
+5	0.045	27%	41%
+10	0.00015	25%	50%
+10	0.0015	29%	46%
+10	0.015	21%	37%
+10	0.045	19%	31%
+20	0.00015	33%	40%
+20	0.0015	19%	32%
+20	0.015	14%	22%
+20	0.045	8%	14%

takes into account the effect of natural convection in the melt layer of the PCM. An experimental test unit was constructed and the numerical predictions were verified against experimental data. A series of numerical experiments were then undertaken to assess the effects of the shell radius, of the mass flow rate and inlet temperature of the HTF, and of the presence of annular fins attached to the inner tube on the thermal behavior of the storage unit. Results showed that the annular fins are most effective for moderate mass flow rates ($0.0015 \text{ kg s}^{-1} \leqslant \dot{m} \leqslant 0.015 \text{ kg s}^{-1}$) and small inlet temperatures ($\Delta T_{in} = +5 \text{ K}$).

Acknowledgements—The author expresses his gratitude to the Natural Sciences and Engineering Council of Canada for the financial support that enables him to conduct this work.

REFERENCES

1. N. Shamsundar and R. Srinivasan, Effectiveness NTU charts for heat recovery from latent heat storage units. *J. Solar Energy Engng* **102**, 263–271 (1980).
2. D. J. Morrison and S. I. Abdel-Khalik, Effects of phase-change energy storage on the performance of air-based and liquid-based solar heating systems, *Sol. Energy* **20**, 57–67 (1978).
3. N. Shamsundar and R. Srinivasan, Analysis of energy storage by phase change with an array of cylindrical tubes, ASME Winter Annual Meeting, San Francisco (1978).
4. K. A. R. Ismail and C. L. F. Alves, Analysis of shell-and-tube PCM storage system, *Proceedings of the 8th International Heat Transfer Conference*, San Francisco, U.S.A., pp. 1781–1786 (1986).
5. B. Yimmer and M. Adami, Parametric study and optimization of phase change thermal energy storage systems, *National Heat Transfer Conference, HTD*, Vol. 109, *Multiphase Flow, Heat and Mass Transfer*, pp. 1–8 (1989).
6. E. Hahne, Thermal energy storage: some views on some problems, *Proceedings of the 8th Int. Heat Transfer Conference*, San Francisco, pp. 279–292 (1986).
7. K. Sasaguchi, M. Yoshida and S. Nakashima, Heat transfer characteristics of a latent heat thermal energy storage unit with a finned tube (effects of fin configuration). *Trans. JSME* **54**(504), 2136–2143 (1988).
8. K. Sasaguchi, Heat-transfer characteristics of a latent heat thermal energy storage unit with a finned tube. *Trans. JSME* **55**(510), 475–482 (1989).
9. P. V. Padmanabhan and M. V. K. Murthy, Outward phase change in a cylindrical annulus with circumferential fins, *Proceedings of the 8th Int. Heat Transfer Conference*, San Francisco, pp. 1773–1779 (1986).
10. J. Eftekhar, A. Haji-Sheikh and D. Y. S. Lou, Heat transfer enhancement in a paraffin wax thermal storage system. *J. Solar Energy Engng* **106**, 299–306 (1984).
11. H. Rieger, U. Projahn and H. Beer, Analysis of the heat transport mechanisms during melting around a horizontal circular cylinder, *Int. J. Heat Mass Transfer* **25**, 137–147 (1982).
12. M. M. Farid and R. M. Hussian, An electrical storage heater using the phase-change method of heat storage, *Energy Conser. Mgmt* **30**(3), 219–230 (1990).
13. J. Crank, *Free and Moving Boundary Problems*. Clarendon Press, Oxford (1984).
14. V. R. Voller, Fast implicit finite-difference method for the analysis of phase change problems, *Numer. Heat Transfer, Part B* **17**, 155–169 (1990).
15. S. Kakac, R. K. Shah and W. Aung, *Handbook of Single Phase Convective Heat Transfer*, pp. 3–21. Wiley, New York (1986).
16. F. P. Incropera and D. P. De Witt, *Fundamentals of Heat and Mass Transfer*, p. 496. Wiley, New York (1990).